THE JOURNAL OF BIOLOGICAL CHEMISTRY VOL. 287, NO. 14, pp. 11489–11497, March 30, 2012

Successful Prediction of Substrate-binding Pocket in SLC17 Transporter Sialin*[S]

Received for publication, October 12, 2011, and in revised form, February 4, 2012 Published, JBC Papers in Press, February 13, 2012, DOI 10.1074/jbc.M111.313056

Nicolas Pietrancosta[‡1], Christine Anne[§1], Horst Prescher[¶], Raquel Ruivo[§‖], Corinne Sagné[§], Cécile Debacker[§], Hugues-Olivier Bertrand[**], Reinhard Brossmer[‡‡], Francine Acher[‡], and Bruno Gasnier[§2]

*From the [‡]Centre National de la Recherche Scientifique, UMR 8601 and [§]Centre National de la Recherche Scientifique, UMR 8192, Université Paris Descartes, Sorbonne Paris Cité, F-75006 Paris, France, [¶]G3-BioTec, D-69207 Sandhausen, Germany, the [‖]Graduate School ED 419, Université Paris-Sud, F-94276 Le Kremlin-Bicêtre, France, **Accelrys, Parc Club Orsay Université, F-91898 Orsay Cedex, France, and the [‡‡]Biochemistry Center, University of Heidelberg, D-69120 Heidelberg, Germany*

Background: Sialin is a clinically relevant lysosomal sialic acid exporter related to vesicular glutamate transporters and other SLC17 transporters.
Results: Using synthetic sialic acid analogues, homology modeling, site-directed mutagenesis, and virtual screening, we built and validated a three-dimensional model of sialin.
Conclusion: The three-dimensional model successfully predicts small molecule binding to sialin.
Significance: The model will help identifying pharmacological tools targeted to SLC17 transporters.

Secondary active transporters from the SLC17 protein family are required for excitatory and purinergic synaptic transmission, sialic acid metabolism, and renal function, and several members are associated with inherited neurological or metabolic diseases. However, molecular tools to investigate their function or correct their genetic defects are limited or absent. Using structure-activity, homology modeling, molecular docking, and mutagenesis studies, we have located the substrate-binding site of sialin (SLC17A5), a lysosomal sialic acid exporter also recently implicated in exocytotic release of aspartate. Human sialin is defective in two inherited sialic acid storage diseases and is responsible for metabolic incorporation of the dietary nonhuman sialic acid *N*-glycolylneuraminic acid. We built cytosol-open and lumen-open three-dimensional models of sialin based on weak, but significant, sequence similarity with the glycerol-3-phosphate and fucose permeases from *Escherichia coli*, respectively. Molecular docking of 31 synthetic sialic acid analogues to both models was consistent with inhibition studies. Narrowing the sialic acid-binding site in the cytosol-open state by two phenylalanine to tyrosine mutations abrogated recognition of the most active analogue without impairing neuraminic acid transport. Moreover, a pilot virtual high-throughput screening of the cytosol-open model could identify a pseudopeptide competitive inhibitor showing >100-fold higher affinity than the natural substrate. This validated model of human sialin and sialin-guided models of other SLC17 transporters should pave the way for the identification of inhibitors, glycoengineering tools, pharmacological chaperones, and fluorescent false neurotransmitters targeted to these proteins.

The major facilitator superfamily (MFS)[3] (1, 2) is the largest group of secondary active transporters and is responsible for the passive (uniporters) or active transport of a wide diversity of substrates, including inorganic ions, sugars, amino acids, and xenobiotics, across cellular and intracellular membranes in all kingdoms of life. MFS proteins typically contain 12 transmembrane helices (TM), divided in two six-TM halves surrounding a central aqueous cavity containing the substrate-binding site. Rigid body rotation of the N- and C-terminal halves alternately opens the central binding site on one side of the membrane or the other (1, 3, 4). This "rocker switch" mechanism ensures "uphill" transport of substrate when it is coupled to "downhill" transport of driving ions such as Na^+ or protons.

The human SLC17 protein family encodes a subgroup of anion transporters within the MFS, which includes the type I Na^+/phosphate transporter (NPT1) and three related proteins, three vesicular glutamate transporters (VGLUT1–3), a vesicular nucleotide transporter (VNUT), and sialin (5, 6). NPT1 and NPT4 are renal and liver transporters for diverse organic anions, including urate, which have been associated with increased risk of gout (7–9). VGLUTs accumulate glutamate into synaptic vesicles (5), whereas VNUTs accumulate ATP into secretory organelles (6). A VGLUT3 missense mutation has been associated with an autosomal-dominant form of progressive deafness (10). Finally, sialin (*SLC17A5* gene) exports hydrolysis-derived *N*-acetylneuraminic acid (Neu5Ac) and acidic hexoses from lysosomes (11, 12). The latter process is defective in two rare lysosomal storage diseases caused by *SLC17A5* mutations: infantile sialic acid storage disease and Salla disease (13, 14). Infantile sialic acid storage disease is an

* This work was supported by the Centre National de la Recherche Scientifique and by a transdisciplinary grant from Université Paris Descartes (to N. P. and B. G.).
[S] This article contains supplemental methods, Table S1, and Figs. S1–S6.
[1] Both authors contributed equally to this work.
[2] To whom correspondence should be addressed: Centre National de la Recherche Scientifique, UMR 8192, Université Paris Descartes, Sorbonne Paris Cité, 45 rue des Saints-Pères, F-75006 Paris, France. Tel.: 33-7064-9915; Fax: 33-7064-9913; E-mail: bruno.gasnier@parisdescartes.fr.

[3] The abbreviations used are: MFS, major facilitator superfamily; GlpT, glycerol-3-phosphate transporter; HTS, high-throughput screening; Neu5Ac, *N*-acetylneuraminic acid; Neu5Gc, *N*-glycolylneuraminic acid; NPT, Na^+/phosphate transporter; TM, transmembrane helix; VGLUT, vesicular glutamate transporter; VNUT, vesicular nucleotide transporter; per-*O*-Ac,9-iodo-Neu5Ac, 9-deoxy-9-iodo-2,4,7,8-tetra-*O*-acetyl-Neu5Ac; per-*O*-Pr,9-iodo-Neu5Ac, 9-deoxy-9-iodo-2,4,7,8-tetra-*O*-propanoyl-Neu5Ac.

early-lethal, multisystemic disease associated with diverse deletions, insertions, and missense and nonsense mutations, whereas Salla disease is a progressive, nonlethal leukodystrophy almost exclusively associated with the specific mutation R39C. There is no effective treatment. In contrast with infantile sialic acid storage disease missense mutations, R39C partially preserves sialic acid transport, thus accounting for the lesser severity of Salla disease (11, 12). On the other hand, R39C strongly impairs the trafficking of sialin to lysosomes (11, 15), thus offering a potential therapeutical approach to rescue the intracellular localization of the partially active mutant using pharmacological chaperones (16).

Recently, flux studies in proteoliposomes have shown that sialin accumulates glutamate and, in contrast with VGLUTs, aspartate into positively charged vesicles, in addition to its sialic acid export function. Sialin thus probably represents the long sought for vesicular transporter underlying aspartate neurotransmission (17). However, physiological evidence is still needed to firmly establish this conclusion. As mutation R39C abolished aspartate transport, this additional function of sialin may contribute to the pathophysiology of Salla disease (17).

Another clinically important aspect of sialin is that it is the sole known route for the cell entry of exogenous sialic acids, including the dietary sialic acid *N*-glycolylneuraminic acid (Neu5Gc), through a two-step process involving fluid-phase endocytosis followed by lysosomal export (18). As humans are genetically deficient in Neu5Gc synthesis, this results in the production of anti-Neu5Gc antibodies that contribute to chronic inflammation and enhanced tumor progression (19). The metabolic incorporation of Neu5Gc also alters cell-cell and cell-pathogen interactions that depend on surface sialoglycoconjugates (20).

Despite these diverse essential roles, the pharmacology of SLC17 transporters is extremely limited. Sialin interacts with sialic acids and aspartate in the millimolar range, and no effective inhibitor has been documented. Competitive and noncompetitive inhibitors have been identified for VGLUTs with affinities reaching into the nanomolar range (21–23). However, their use is limited to *in vitro* studies because most are membrane-impermeant, and their selectivity is limited. High-throughput screening (HTS) of drugs is thus needed to investigate further the mechanism and physiological functions of SLC17 transporters. In this study, we characterized the sialic acid-binding site of sialin using structure-activity relationships, homology modeling, and molecular docking techniques. We synthesized and characterized over 30 unnatural sialic acids and, in parallel, built two three-dimensional homology models of sialin based on bacterial MFS transporters crystallized in the two alternate states of the rocker switch mechanism (4, 24). The homology models were further used for computational docking of the sialic acid analogues, and the cytosol-open model was validated using site-directed mutagenesis. We then demonstrated the feasibility of virtual HTS in a pilot study.

EXPERIMENTAL PROCEDURES

Chemicals—*N*-Acetylneuraminic acid (Neu5Ac) was obtained from Sigma-Aldrich. *N*-Acetyl [6-^{3}H]neuraminic acid (20 Ci/mmol) was from American Radiolabeled Chemicals (St. Louis, MO). FR139317 (*N*-[*N*-[*N*-[(hexahydro-1*H*-azepin-1-yl)carbonyl]-L-leucyl]-l-methyl-D-tryptophyl]-3-(2-pyridinyl)-D-alanine) (three batches; all bioactive) was from Sigma-Aldrich and from Tocris Biosciences (Bristol, UK).

The following sialic acid analogues were synthesized as described previously: Neu5Ac-per-*O*-acetyl (25); Neu5Ac-methylester (26); Neu5Ac-methylester-per-*O*-acetyl (26); β-methyl-Neu5Ac (26); 2,3-dehydro-Neu5Ac (27); α-methyl-Neu5Ac (25); 4-oxo-Neu5Ac (28); 4-deoxy-Neu5Ac (29, 30); 4-*O*-acetyl-Neu5Ac (31); Neu5Ac-4-oxime (32); Neu5N-propanoyl (33); Neu5N-trifluoracetyl (34–36); Neu5N-fluoracetyl (37); Neu5N-butanoyl (33); 9-deoxy-9-iodo-Neu5Ac (38); 9-deoxy-9-methylthio-Neu5Ac (38); 9-deoxy-9-thio-Neu5Ac (39); 9-deoxy-9-azido-Neu5Ac (36, 40, 41); 9-deoxy-Neu5Ac (42); 9-deoxy-9-acetylamino-Neu5Ac (36, 43); 9-*O*-methyl-Neu5Ac (44, 45); 9-deoxy-9-amino-Neu5Ac (43); 9-deoxy-9-benzoylamino-Neu5Ac (36, 43); and 9-deoxy-9-iodo-Neu5Ac methylester (63). 9-Deoxy-9-iodo-2,4,7,8-tetra-*O*-acetyl-Neu5Ac (per-*O*-Ac,9-iodo-Neu5Ac); 9-deoxy-9-iodo-2,4,7,8-tetra-*O*-propanoyl-Neu5Ac (per-*O*-Pr,9-iodo-Neu5Ac); 9-deoxy-9-thioisopropyl-Neu5Ac; 9-deoxy-9-nitro-Neu5Ac; 9-deoxy-9-methylsulfoxido-Neu5Ac; and 9-deoxy-9-iodo-Neu5Ac-4,7,8-tri-*O*-methy were synthesized and characterized by high-resolution mass spectroscopy and NMR (^{1}H and ^{13}C) as described in the supplemental Methods. Stock solutions of compounds (100 mM) were made in aqueous medium, except for per-*O*-Pr,9-iodo-Neu5Ac and FR139317, which were dissolved in dimethyl sulfoxide (DMSO).

Site-directed Mutagenesis—Missense mutations were introduced into EGFP-tagged, L22G/L23G human sialin (11) using QuikChange site-directed mutagenesis (Stratagene, La Jolla, CA), and primers are listed in supplemental Table S1. The whole coding sequence was verified by automated sequencing. The construct without additional mutation is referred to as "wild-type."

Sialic Acid Transport—[^{3}H]Neu5Ac uptake was measured in whole HEK-293 cells expressing recombinant human sialin at their plasma membrane as described (11), with minor changes. HEK-293 cells (300,000/well in poly-D-lysine-coated 24-well plates) were grown at 37 °C under 5% CO_2 in glucose-rich Dulbecco's modified Eagle's medium supplemented with penicillin, streptomycin, and 10% fetal bovine serum. Transfection was performed using Lipofectamine 2000 (Invitrogen). [^{3}H]Neu5Ac uptake was measured in triplicate in whole cells expressing recombinant human sialin at their plasma membrane. Cells were incubated for 15 min at room temperature with [^{3}H]Neu5Ac (0.1 μCi/well) in a medium buffered with MES-Na^+, pH 5.0. After washes in ice-cold medium, the radioactivity in the cells was counted by liquid scintillation. Inhibitors were added simultaneously with [^{3}H]Neu5Ac. For saturation kinetics, incubation was shortened to 10 min to keep measurements within the linear phase of uptake at all [^{3}H]Neu5Ac concentrations.

Results are expressed as means ± S.E. from *n* independent experiments. IC_{50} and kinetic parameter values were derived by nonlinear regression of untransformed data using the SigmaPlot 8.0 software (Systat Software, Inc.). Linear regression in

Fig. 5*D* yielded similar values. Statistical comparisons were made using paired *t* test and Mann-Whitney test.

Homology Modeling—Secondary structures were predicted using TMHMM (46) and HMMTOP (47). Sequence alignments were generated between human sialin (SWISS-PROT accession number Q9NRA2), on one hand, and glycerol-3-phosphate transporter (GlpT) (P08194) or fucose permease (P11551), on the other hand, using Clustal W (10). Alignments were manually refined to avoid gaps in predicted (human sialin) and known (GlpT and fucose permease) secondary structure elements. Three-dimensional sialin models were built from these alignments and from crystallographic atomic coordinates of GlpT (Protein Data Bank (PDB) ID: 1PW4) and fucose permease (PDB ID: 3O7Q) using the automated comparative modeling tool MODELER 9.0 (Discovery Studio 2.5.5, Accelrys Software Inc., San Diego CA).

Molecular Docking—All calculations were performed in Discovery Studio 2.5.5. Flexible ligand-rigid protein docking was performed using CDOCKER (48). Random ligand conformations were generated from the initial ligand structure through high-temperature molecular dynamics. Due to the high flexibility of sialic acids, we docked for each ligand several conformations previously generated with the BEST algorithm (49) to cover the full range of conformers. The poses showing the lowest energy were retained and clustered according to their binding mode. Three-dimensional snapshots of the docked ligands were generated using Accelrys DS Visualizer. Residues involved in ligand-protein interaction were displayed using the LigPlot program (50). Ramachandran plots were performed as described (51). Virtual high-throughput screening was performed similarly using chemical structures from the ZINC database (52).

RESULTS

Structure-Activity Relationship of Sialic Acid Analogues—As a first step to characterize the sialic acid binding activity of human sialin, we characterized its interaction with synthetic analogues of Neu5Ac. Over 30 compounds were synthesized by changing substituents at carbons 1, 2, 4, 5, or 9 in the Neu5Ac scaffold (Fig. 1*A*). Some analogues were modified at all hydroxyl groups (per-*O*-esterified analogues). Substituents were chosen to alter potential protein-ligand interactions or induce steric hindrance in the binding pocket. The compounds were tested for their capacity to inhibit [^{3}H]Neu5Ac uptake in a whole-cell functional assay where the poorly accessible lysosomal efflux is replaced by a cellular influx (11). Experiments were performed at extracellular pH 5.0 to mimic the acidic environment of the lysosomal lumen. To maximize detection of differences relative to Neu5Ac, compounds were first tested at 1 mM, a concentration at which Neu5Ac half-inhibits uptake (Fig. 1*B*). Bioactive compounds available in sufficient amounts were further characterized in dose-response curves (Table 1).

Esterification of the carboxylic group at position 1 (R_1) and suppression or methylation of the hydroxyl group at position 2 (R_2) decreased recognition, suggesting that these two groups interact with the sialic acid-binding pocket. Modification at position 4 or 9 altered recognition, with the highest increases observed when the hydroxyl group at position 9 was replaced by a thiol, a methylthio, or an iodine group (Fig. 1*B*). Among mono-substituted compounds, the best analogue was 9-iodo-Neu5Ac, which inhibited [^{3}H]Neu5Ac uptake with a half-max-

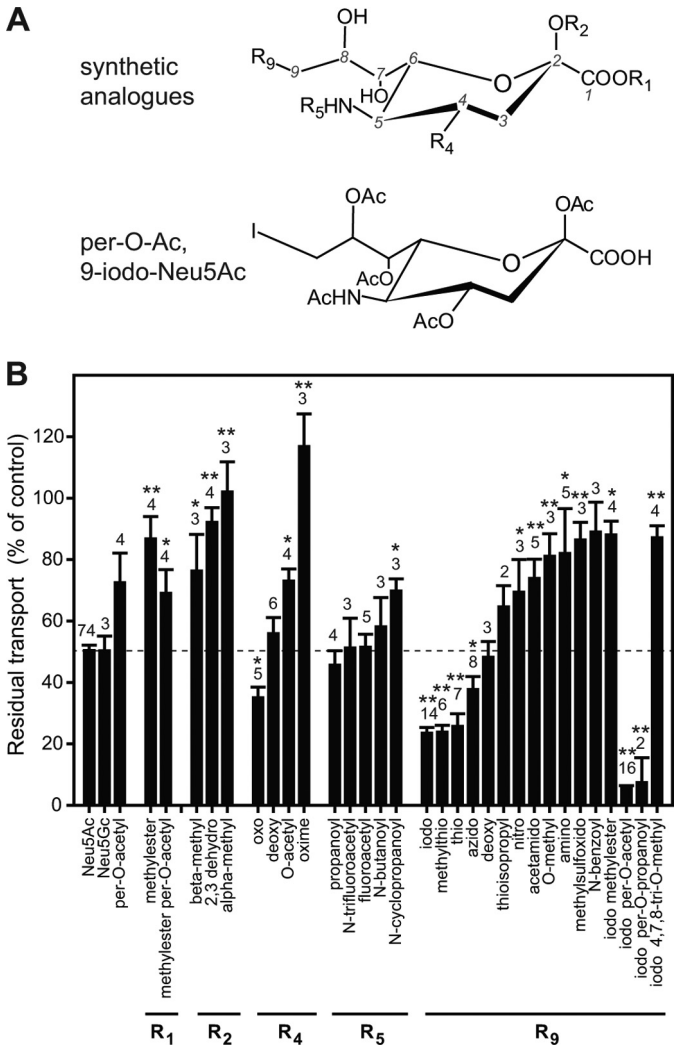

FIGURE 1. **Structure-activity relationship of human sialin.** *A*, a generic synthetic sialic acid analogue (*top structure*) and the most bioactive analogue, per-*O*-Ac,9-iodo-Neu5Ac, are shown under their β anomeric state. The nine carbon atoms of the Neu5Ac scaffold are *numbered* in *italics*. *B*, inhibition of [^{3}H]Neu5Ac uptake by synthetic analogues (1 mM) at pH 5.0. The *dotted line* shows inhibition by unlabeled Neu5Ac. The *numbers* and *asterisks* above the bars indicate numbers of independent experiments and the statistical significance (Mann-Whitney test). *, $p < 0.05$; **, $p < 0.001$.

TABLE 1

IC_{50} of the synthetic sialic acid analogues for wild-type sialin

[^{3}H]Neu5Ac uptake into whole HEK-293 cells expressing human sialin at their plasma membrane was measured at pH 5.0 in the presence of increasing concentrations of the tested compound. IC_{50} values were derived by nonlinear regression of the dose-response curves. Results are means ± S.E. from *n* independent experiments; ND, not determined.

Compound	IC_{50}	Ratio to Neu5Ac in paired measurement (*x*-fold)	*n*
	μM		
Neu5Ac	902 ± 107	1	26
4-Oxo-Neu5Ac	429 ± 125	1.6 ± 1.3	3
5-Fluoroacetyl-Neu5Ac	540	1.3	1
9-Azido-Neu5Ac	542 ± 8	1.2 ± 0.2	2
9-Iodo-Neu5Ac	243 ± 77	3.1 ± 0.8	4
9-Methylthio-Neu5Ac	324	1.4	1
9-Thio-Neu5Ac	604 ± 309	0.93 ± 0.5	2
Per-O-Ac,9-iodo-Neu5Ac	40.7 ± 6.0	39.5 ± 11.8	12
Per-O-Pr,9-iodo-Neu5Ac	68	ND	1

imal inhibitory concentration (IC_{50}) of 243 ± 77 μM (n = 4), representing an ~3-fold improvement over Neu5Ac (Table 1). Analogue recognition was further improved when the remaining free hydroxyl groups of 9-iodo-Neu5Ac were conjugated to acetyl or propanoyl groups, but not methyl groups, thus suggesting that insertion of carbonyls at positions 2, 4, 7, and 8 was responsible for the increased interaction with sialin. In striking contrast, per-*O*-acetylation of Neu5Ac did not improve recognition, an apparent paradox that can be explained if the presence of an acetyl group at position 9 weakens binding, as do for instance acetamido and *O*-methyl substituents (Fig. 1*B*). Single *O*-acetylation of Neu5Ac at position 4 also impaired recognition, suggesting that carbonyl groups at positions 2, 7, and 8 predominate in the strong affinity of per-*O*-Ac,9-iodo-Neu5Ac for human sialin (IC_{50} = 41 ± 6 μM, representing an ~40-fold improvement over Neu5Ac). Modification of the substituent at position 5, including that found in Neu5Gc, had no effect. However, because the amide bond was preserved in these analogues, an interaction of the carbonyl group or the nitrogen atom with sialin cannot be excluded.

It should be noted that our experiments could not discriminate between α and β anomers, either because they were subjected to dynamic anomerization equilibrium or because the anomers could not be separated after synthesis when this equilibrium was blocked (R_2 substitutions, including per-*O*-esterifications). The sole exception was 2-methyl Neu5Ac, which could be tested separately as α and β anomers. We found that β-2-methyl Neu5Ac was a better inhibitor than the α anomer (48 ± 9 and 90 ± 9% residual uptake, respectively, at 10 mM inhibitor; p = 0.002). These data suggest that Neu5Ac is recognized under its predominant (β) anomeric state, but recognition of α anomers cannot be excluded for more substituted analogues.

Molecular Modeling of Sialin—In an independent line of investigation, we built three-dimensional models of human sialin using crystallographic MFS transporter structures as templates. A BLAST search against the PDB from the Research Collaboratory for Structural Bioinformatics identified the GlpT from *E. coli* (PDB ID: 1PW4) (24) as the most homologous template (18% of sequence identity; 40% of sequence similarity). Until recently, all MFS transporters, including GlpT, had been crystallized in a cytosol-open conformation (3, 24) or, for the hydrophobic drug exporter EmrD, in a conformation open to the cytosolic leaflet of the membrane (53). However, an opposite outward-open conformation (PDB ID: 3O7Q) was crystallized during the course of this study for the *E. coli* fucose permease (16% of sequence identity and 36% of sequence similarity with human sialin) (4). As exogenously added ligands first interact with this outward-open conformation in our whole-cell assay, the fucose permease structure prompted us to build a second three-dimensional model of human sialin open to the lysosomal lumen. Quality control analysis identified only four and five non-glycine, non-proline residues (0.9 and 1.1% of the primary structure) in forbidden areas of Ramachandran diagrams derived from the GlpT-based and fucose permease-based models, respectively.

In Silico Docking Identifies Best Synthetic Analogues—Next, we docked in silico the synthetic analogues to the lumen-open and cytosol-open models to assess their consistency with experimental data. Because the analogue anomeric state could not be controlled (see above), both α and β anomers were docked, except for the natural substrate Neu5Ac, which was docked under its predominant β anomer. The outcome of these calculations is summarized in Fig. 2, where compounds are plotted according to their global docking energy and their actual bioactivity in the uptake assay. Interestingly, the same subset of four compounds stood out as the best docked molecules regardless of the anomeric state and sialin model, and this subset included the two best inhibitors of the transport assay: per-*O*-Ac,9-iodo-Neu5Ac and per-*O*-Pr,9-iodo-Neu5Ac. The top subset also included two weak inhibitors (per-*O*-Ac,Neu5Ac and per-*O*-Ac,Neu5Ac methylester), an unsurprising finding as computational docking is known to generate false positives (54). Overall, these data suggest that both three-dimensional models capture the key features characterizing the interaction of sialic acids with human sialin.

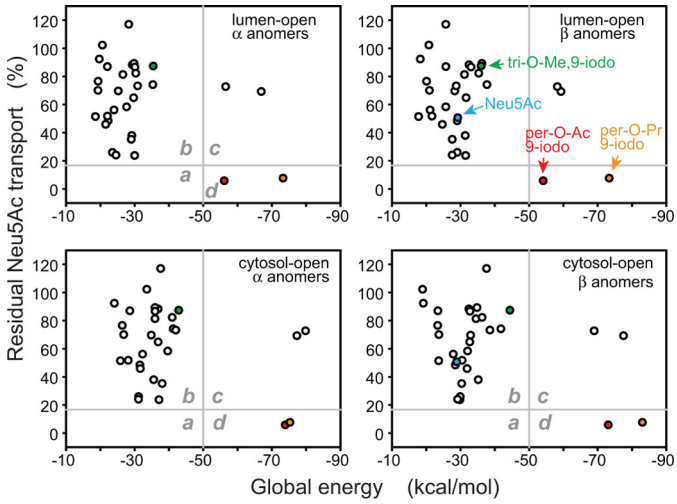

FIGURE 2. **Molecular docking of sialic acid analogues to lumen-open and cytosol-open sialin models.** Synthetic analogues were docked *in silico* to the three-dimensional models under their α or β anomeric state. Residual transport levels shown in Fig. 1*B* were plotted against the global energy of the most stable ligand-protein pose for each compound. The *horizontal gray line* corresponds to a 5-fold increase in affinity relative to Neu5Ac. The *vertical line* was positioned to separate top-scoring docked compounds from medium- and low-scoring compounds. Quadrants *a*, *b*, *c*, and *d* correspond to false negative, true negative, false positive, and true positive hits, respectively.

The best poses for α- and β-per-*O*-Ac,9-iodo-Neu5Ac docked to the lumen-open and cytosol-open models are illustrated in Fig. 3 and supplemental Figs. S1 and S2. In these different poses, the synthetic analogue makes numerous polar and nonpolar interactions with side chains present in TMs 1, 2, 4, 5, 7, 10, and 11. In the lumen-open model, the analogue carboxylic group forms a hydrogen bond with Asn-430 in TM11 (both anomers), as well as hydrogen (Tyr-301, Asn-302) and ionic (His-298) bonds with TM7 residues in the case of the β anomer. Additional hydrogen bonds from Tyr-54, Tyr-203, Tyr-119, His-183, and Tyr-306 to carbonyl groups of the acetyl substituents, as well as numerous van der Waals interactions between nonpolar residues and the methyl groups of these acetyls, stabilize docking. In the cytosol-open model, the analogue carboxylic group makes hydrogen and ionic bonds with Tyr-54 and Arg-57 in TM1 and Tyr-119 in TM2 (both anomers), instead of

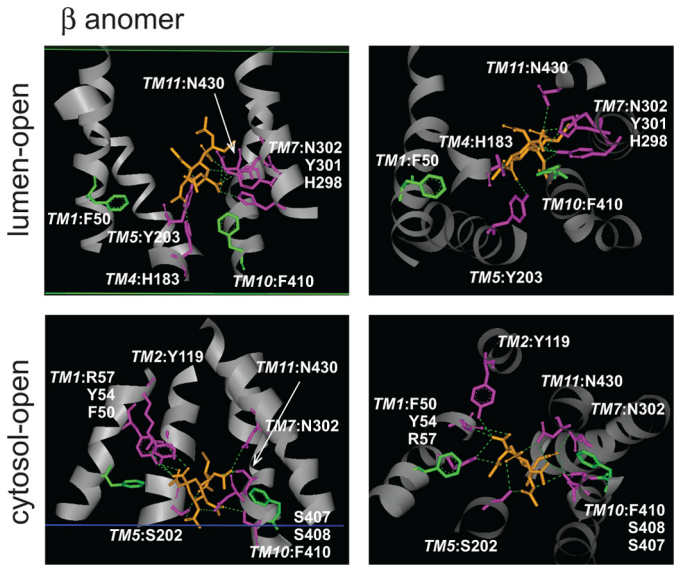

FIGURE 3. **Structural snapshots of β anomer of per-*O*-Ac,9-iodo-Neu5Ac docked into its binding pocket.** Lumen-open and cytosol-open sialin models are shown in the *top* and *bottom* rows, respectively. *Left images* are side views, with the lysosomal lumen (equivalent to the extracellular compartment in our transport assay) at the *top*. *Green* and *blue continuous lines* indicate luminal and cytosolic boundaries of the membrane, respectively. *Right images* are views from the cytosol. For clarity, only residues having polar interactions with the ligand (*pink side chains*) are displayed, along with two phenylalanine residues (*green*) subjected to mutagenesis in Fig. 4. *Dotted green lines* indicate hydrogen bonds.

TMs 7 and 11. Additional hydrogen bonds from Tyr-54, Ser-202, Asn-302, Ser-407, Ser-408, Ser-411, and Asn-430 to the carbonyl groups and ester oxygen atoms of the analogue, as well as numerous nonpolar interactions, contribute to high-affinity binding.

Missense Mutation of Phe-50 and Phe-410 Selectively Abolishes High-affinity Recognition of Best Sialic Acid Analogue—To test the relevance of the docking models, we selected residues interacting with per-*O*-Ac,9-iodo-Neu5Ac, but not Neu5Ac, and examined whether mutation of these residues could impair analogue recognition while preserving Neu5Ac uptake. We initiated this mutagenesis study on the earlier built, cytosol-open model. Two phenylalanine residues (Phe-50 and Phe-410 in TMs 1 and 10, respectively) making van der Waals contacts on diametrically opposite sides of α- and β-per-*O*-Ac,9-iodo-Neu5Ac were selected (Fig. 4*A*) as they provided a sort of "molecular caliper" to verify the docking accuracy (we deliberately ignored anomer-specific interactions because we could not discriminate anomers in "wet" experiments). We reasoned that narrowing the molecular caliper by replacing the para-proton by a hydroxyl group at the extremity of these side chains (F50Y and F410Y mutations) should cause steric hindrance, disrupt the hydrophobic environment, and selectively impair per-*O*-Ac,9-iodo-Neu5Ac binding. On the other hand, ablating the phenyl side chains (F50A, F410A) should have a minor effect because numerous van der Waals interactions contribute to docking in addition to those made by Phe-50 and

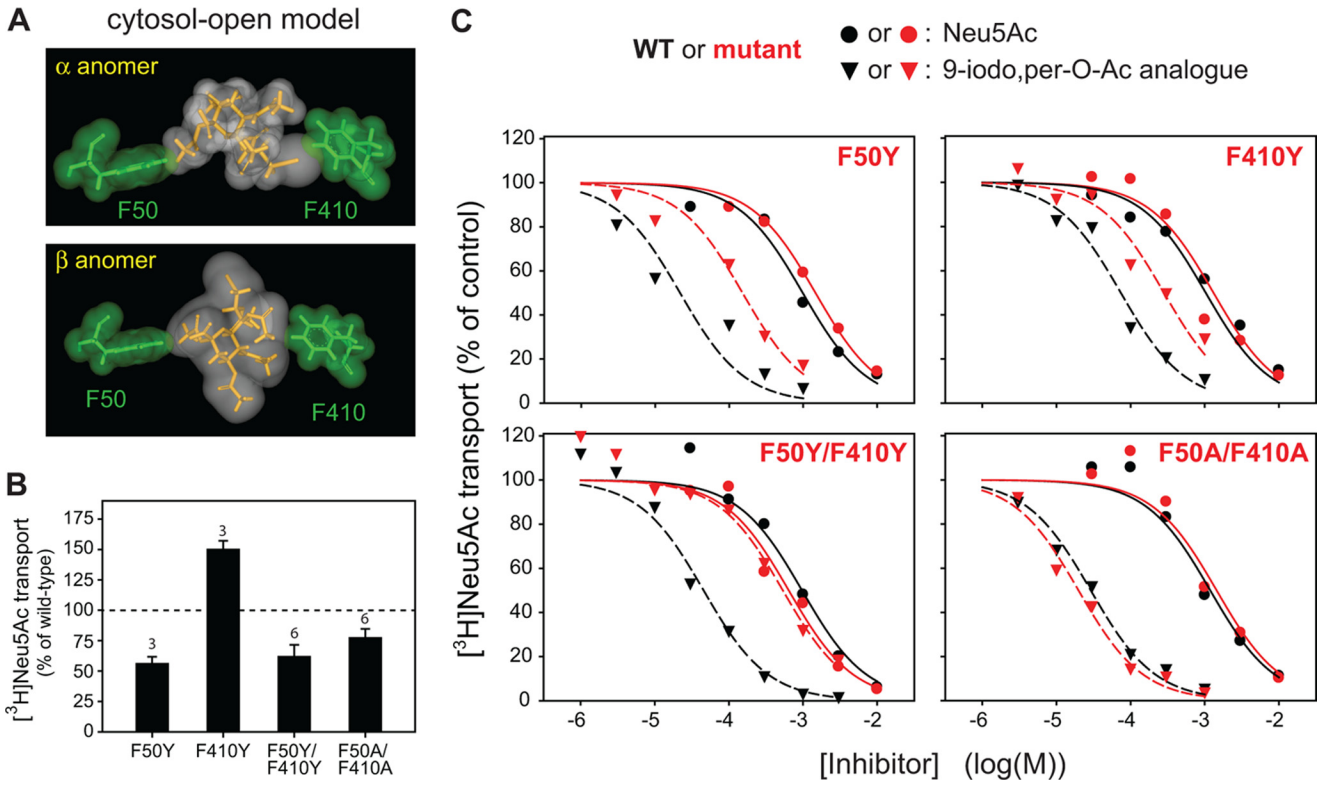

FIGURE 4. **Narrowing sialic acid-binding pocket of sialin by conservative missense mutations selectively impairs recognition of synthetic analogue per-*O*-Ac,9-iodo-Neu5Ac.** *A*, space-filling models of the docked analogue (*yellow*) and of Phe-50 and Phe-410 side chains (*green*) show that the two phenylalanines make van der Waals contacts with the ligand in the cytosol-open state of human sialin. This holds true for both α and β anomers despite their distinct positions in the binding pocket. *B*, single and double missense mutants of Phe-50 and Phe-410 show substantial Neu5Ac transport activity. The *number* above the bars indicate numbers of independent experiments. *C*, dose-response inhibition curves of wild-type (*black*) and mutant (*red*) sialin by Neu5Ac (*circles*) and the synthetic analogue (*triangles*). Representative experiments are shown. See Table 2 for average results from independent experiments.

TABLE 2

IC_{50} values of the sialin mutants

[^{3}H]Neu5Ac uptake was measured at pH 5.0 in the presence of increasing concentrations of Neu5Ac or synthetic analogue using HEK-293 cells expressing the tested sialin mutant at their plasma membrane. Results are means ± S.E. from *n* independent experiments.

Sialin construct	Neu5Ac (*n*)	Per-O-Ac,9-iodoNeu5Ac (*n*)
	μM	μM
Wild-type	1280 ± 140 (12)	38 ± 5 (12)
F50Y	1380 ± 80 (2)	270 ± 120 (2)
F410Y	830 ± 170 (2)	220 ± 70 (2)
F50Y/F410Y	1300 ± 340 (3)	500 ± 40 (2)
F50A/F410A	1270 ± 280 (4)	21 ± 3 (4)

Phe-410. Docking simulations using the corresponding sialin mutants corroborated these predictions and the lack of expected effect on Neu5Ac recognition (supplemental Fig. S3).

Fig. 4, *B* and *C*, and Table 2 show the outcome of the mutations in wet experiments. All mutants translocated [^{3}H]Neu5Ac, thus allowing pharmacological characterization. Strikingly, in excellent agreement with the cytosol-open docking model, the double mutation F50Y/F410Y strongly impaired per-*O*-Ac,9-iodo-Neu5Ac recognition (13-fold IC_{50} increase; paired *t* test, $p = 0.024$), whereas Neu5Ac recognition was not affected. On the other hand, the double mutation F50A/F410A had no significant effect on both compounds, in agreement with the view that steric hindrance of hydroxyl groups in the analogue-binding pocket induces the F50Y/F410Y phenotype. Moreover, the two single mutations F50Y and F410Y caused partial, selective loss of per-*O*-Ac,9-iodo-Neu5Ac recognition (~7- and 6-fold, respectively), thus confirming that the analogue contacts both phenylalanine residues. These data indicate that the GlpT-based, cytosol-open model accurately predicts the position of per-*O*-Ac,9-iodo-Neu5Ac in the binding pocket of human sialin despite its low sequence homology with the GlpT template (19% identity and 45% similarity for residues located within a 6 Å radius of the docked ligand).

By contrast, per-*O*-Ac,9-iodo-Neu5Ac docked to the wild-type lumen-open model showed a gap with the Phe-50 or Phe-410 side chains (supplemental Fig. S4) and, accordingly, docking was not significantly altered by the F50A/F410A and F50Y/F410Y mutations (supplemental Fig. S3). Therefore, the cytosol-open model turned out to be a better predictor of the interaction with per-*O*-Ac,9-iodo-Neu5Ac, although the tested compounds first interact with the lumen-open state in our whole-cell assay. Several possibilities could account for this paradox. (i) Our lumen-open model could be less accurate than the cytosol-open one; (ii) per-*O*-Ac,9-iodo-Neu5Ac could have intrinsically higher affinity for the cytosol-open state and trap sialin in this state; or (iii) the acidic environment facing the lumen-open state in our assay could weaken analogue recognition in this state.

Virtual Screening Identifies Pseudotetrapeptide FR139317 as a Sialin Ligand—To test further the accuracy of the cytosol-open model and assess its practical value, we used it as a template in virtual screening studies to identify novel sialin ligands unrelated to sialic acids. In a pilot study performed on a subset of the ZINC database (52) comprising 12,000 commercially available compounds, we identified 10 compounds (virtual "hits") showing high-affinity docking to cytosol-open sialin. Among these, the top-ranked hit, a pseudotetrapeptide (FR139317; Fig. 5*A*) known as an antagonist of endothelin-A receptors (55), actually inhibited [^{3}H]Neu5Ac uptake with an IC_{50} of 8.0 ± 2.7 μM ($n = 4$), representing ~110- and ~5-fold improvements over Neu5Ac and per-*O*-Ac,9-iodo-Neu5Ac, respectively (Fig. 5*C*). To test whether FR139317 occupies the sialic acid-binding site as predicted by our docking simulations (compare residues involved in Figs. 3 and 5*B*), we performed saturation kinetics experiments in the presence and absence of FR139317 (Fig. 5, *D* and *E*). As expected, the pseudopeptide competitively inhibited [^{3}H]Neu5Ac uptake with a mean inhibitory constant (K_i) of 20.2 ± 6.1 μM ($n = 3$). The increased activity of FR139317 relative to per-*O*-Ac,9-iodo-Neu5Ac may be due to novel polar interactions, in particular with TM8 (Tyr-335), which does not contact the sialic acid analogue, whereas the ionic interaction and most hydrogen bonds are conserved or compensated (Ser-408 by Ser-411; Asn-302 by Tyr-306) (Fig. 5*B* and supplemental Fig. S5).

DISCUSSION

The study of SLC17 transporters and of associated inherited diseases is limited by the lack of pharmacological tools. In this study, we built two three-dimensional homology models of human sialin open to the lysosomal lumen or the cytosol, and we characterized the docking of substrate analogues to these models. Both models were in good agreement with the structure-activity relationship of sialic acids. We further validated the cytosol-open model by reshaping the sialic acid-binding pocket using targeted mutagenesis and demonstrated its practical utility using virtual high-throughput screening.

A major difficulty in homology modeling of SLC17 transporters is their low sequence identity with the bacterial transporters used as templates. It is thus essential to validate the models using mutagenesis and pharmacological approaches. Three homology models of SLC17 transporters have been published thus far for sialin (56), VGLUT2 (57), and VGLUT1 (58). However, only GlpT-based, cytosol-open models were built in these studies and, in the first two, no docking experiments were performed. In the third study, substrates and inhibitors were docked to the VGLUT1 model, and the predicted affinities were in good agreement with experimental data (58). However, the binding sites were not confirmed by mutagenesis, nor exploited by virtual drug screening. Interestingly, the residues equivalent to sialin Phe-50 and Phe-410 are conserved (Phe-73 and Phe-422), and they projected into the central aqueous cavity of the VGLUT1 model, thus implying that TMs 1 and 10 were oriented similarly to our cytosol-open sialin model. However, the conserved arginine of TM9 projected into the central cavity of the VGLUT1 model (Arg-377), but not of our sialin model (Arg-364). Moreover, two binding sites were reported for glutamate and the inhibitor trypan blue in the VGLUT1 model, one in the center of the protein and another at the deep end of the cytosol-open cavity (58), whereas we found a single, central binding site for sialic acids in sialin. Further studies are needed to clarify these discrepancies and determine whether they reflect actual differences between the proteins or modeling errors.

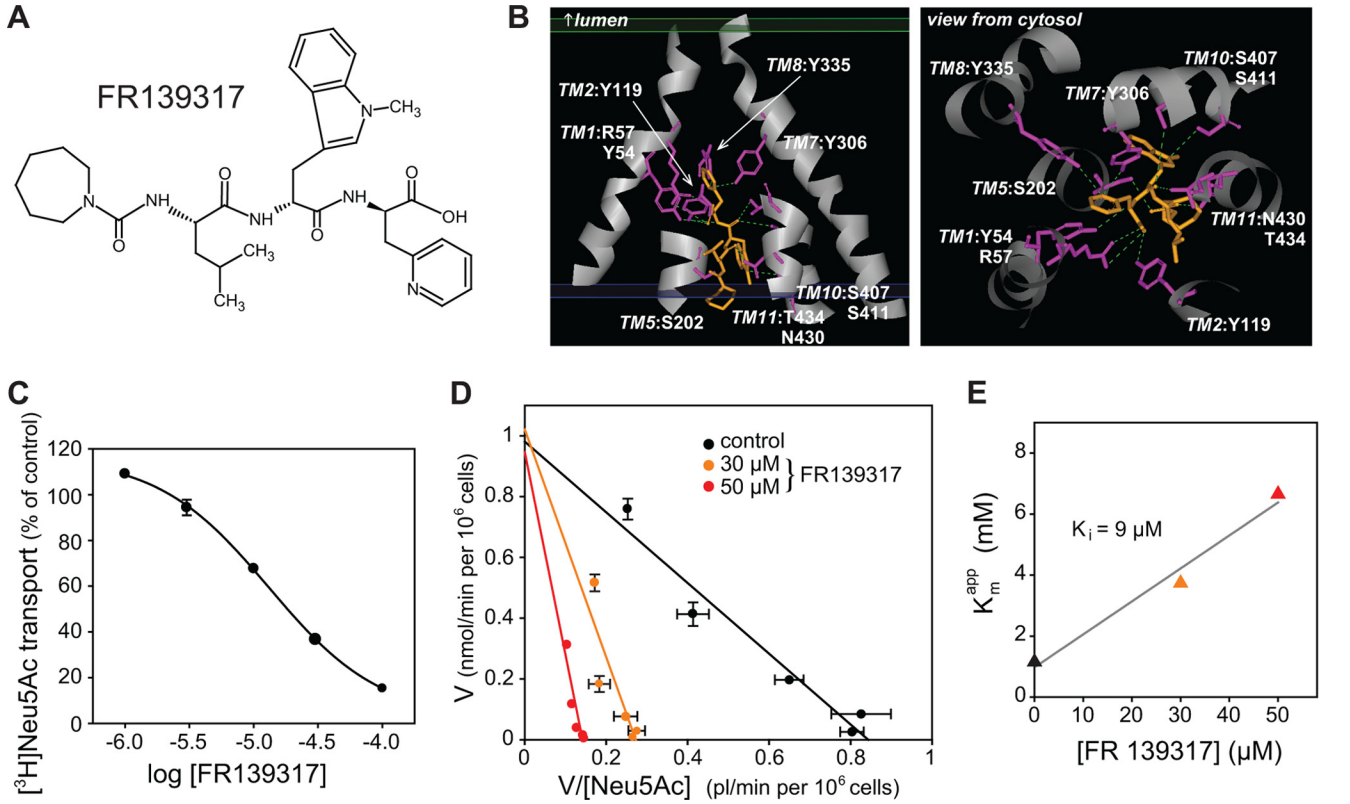

FIGURE 5. **Successful identification of a novel sialin ligand by virtual high-throughput screening.** *A*, chemical structure of the virtual hit. *B*, structural snapshots of FR139317 docked into its binding pocket of the cytosol-open model. Data are displayed as in Fig. 3. Most side chains interacting with the pseudopeptide are also involved in sialic acid analogue binding. *C*, representative dose-response inhibition curve of FR139317. *D*, FR139317 competitively inhibits Neu5Ac uptake. A representative saturation kinetics experiment is shown as an Eadie-Hofstee plot. Where not visible, error bars are smaller than symbols. *E*, the apparent Michaelis-Menten constant (K_m^{app}) derived from regression lines in *D* is plotted as a function of the FR139317 concentration. K_m^{app} increases linearly with this concentration ($r^2 = 0.9776$), yielding an inhibitory constant of 9.0 μM in this experiment.

Surprisingly, our mutagenesis study showed that inhibition by the most bioactive analogue is better predicted by the cytosol-open model (Fig. 4) than the lumen-open model (supplemental Fig. S4), although the compound first interacts with the lumen-open conformation in our functional assay. This suggests that the analogue does not impair the rocker switch mechanism of sialin and that it interacts more strongly with the cytosol-open conformation. As the IC_{50} of per-*O*-Ac,9-iodo-Neu5Ac is in the supramicromolar range, it should eventually dissociate into the cytosol and represent therefore a high-affinity substrate rather than a nontranslocated inhibitor. A similar argument can be made for the pseudopeptide FR139317. Further radiolabeling studies are needed to test these predictions.

Compounds preferentially binding the lumen-open conformation are required to validate more accurately the lumen-open model. To identify such compounds, we synthesized sialic acid analogues larger than per-*O*-Pr,9-iodo-Neu5Ac that presumably should not be accommodated by the rocker switch mechanism; however, their bioactivity could not be determined because of solubility problems. On the other hand, it should be stressed that our lumen-open model is in good agreement with the biochemical demonstration by Courville *et al.* (56) that residues Leu-164 and Phe-179 from TM4 project into the aqueous cavity of the lumen-open conformation and that residue 179 (changed to cysteine in their experiments) is protected from chemical reagents by Neu5Ac binding (supplemental Fig. S5).

Finally, an important milestone of our study is the proof-of-principle demonstration that our validated cytosol-open model is accurate enough to identify unanticipated sialin ligands by virtual drug screening. More comprehensive virtual HTS studies targeted to sialin should provide useful pharmacological tools in the future. Metabolic glycoengineering combined, or not, with bioorthogonal chemistry ("click chemistry") is a powerful approach to modify cell surfaces for a wide range of basic or clinically oriented applications (38, 59–61). However, a practical limitation for *in vivo* experiments is the huge amount of unnatural metabolic precursor (>10 mM) required to substantially enter living cells and modify surface glycoconjugates (59). As this process is mediated by sialin when the precursors are sialic acids (18), virtual screening of unnatural analogue databases should help overcome this bottleneck and, thereby, identify more efficient glycoengineering tools. Virtual HTS studies of broader databases not restricted to sialic acids should provide a variety of molecular tools, such as pharmacological chaperones (16) able to correct the trafficking defect of sialin R39C in Salla disease (11, 15), cell-permeant inhibitors allowing the testing of the proposed aspartatergic role of sialin (17) in a physiological context or, if this role is confirmed, false fluorescent neurotransmitters mimicking the vesicular release of aspartate. The latter compounds are fluorescent substrates used as optical probes to monitor transmitter secretion in cell cultures and brain slices and currently available only for mono-

aminergic neurotransmission (62). As the transport activity of recombinant sialin is easier to test than those of VGLUT and VNUT proteins, the validated sialin models may also guide similar modeling and virtual HTS studies of these vesicular transporters to identify cell-permeant inhibitors and false fluorescent neurotransmitter targeted to glutamatergic and purinergic synapses.

Acknowledgments—We thank E. Kuhfeldt and U. Rose for excellent help with the synthetic work and H. Rudy and T. Timmermann for NMR and MS measurements. We are grateful to Prof. Jäschke and Prof. Fricker for support.

REFERENCES

1. Law, C. J., Maloney, P. C., and Wang, D. N. (2008) Ins and outs of major facilitator superfamily antiporters. *Annu. Rev. Microbiol.* **62,** 289–305
2. Pao, S. S., Paulsen, I. T., and Saier, M. H., Jr. (1998) Major facilitator superfamily. *Microbiol. Mol. Biol. Rev.* **62,** 1–34
3. Abramson, J., Smirnova, I., Kasho, V., Verner, G., Kaback, H. R., and Iwata, S. (2003) Structure and mechanism of the lactose permease of *Escherichia coli*. *Science* **301,** 610–615
4. Dang, S., Sun, L., Huang, Y., Lu, F., Liu, Y., Gong, H., Wang, J., and Yan, N. (2010) Structure of a fucose transporter in an outward-open conformation. *Nature* **467,** 734–738
5. Reimer, R. J., and Edwards, R. H. (2004) Organic anion transport is the primary function of the SLC17/type I phosphate transporter family. *Pflugers Arch.* **447,** 629–635
6. Sawada, K., Echigo, N., Juge, N., Miyaji, T., Otsuka, M., Omote, H., Yamamoto, A., and Moriyama, Y. (2008) Identification of a vesicular nucleotide transporter. *Proc. Natl. Acad. Sci. U.S.A.* **105,** 5683–5686
7. Busch, A. E., Schuster, A., Waldegger, S., Wagner, C. A., Zempel, G., Broer, S., Biber, J., Murer, H., and Lang, F. (1996) Expression of a renal type I sodium/phosphate transporter (NaPi-1) induces a conductance in *Xenopus* oocytes permeable for organic and inorganic anions. *Proc. Natl. Acad. Sci. U.S.A.* **93,** 5347–5351
8. Iharada, M., Miyaji, T., Fujimoto, T., Hiasa, M., Anzai, N., Omote, H., and Moriyama, Y. (2010) Type 1 sodium-dependent phosphate transporter (SLC17A1 protein) is a Cl^--dependent urate exporter. *J. Biol. Chem.* **285,** 26107–26113
9. Dehghan, A., Köttgen, A., Yang, Q., Hwang, S. J., Kao, W. L., Rivadeneira, F., Boerwinkle, E., Levy, D., Hofman, A., Astor, B. C., Benjamin, E. J., van Duijn, C. M., Witteman, J. C., Coresh, J., and Fox, C. S. (2008) Association of three genetic loci with uric acid concentration and risk of gout: a genome-wide association study. *Lancet* **372,** 1953–1961
10. Thompson, J. D., Higgins, D. G., and Gibson, T. J. (1994) CLUSTAL W: improving the sensitivity of progressive multiple sequence alignment through sequence weighting, position-specific gap penalties, and weight matrix choice. *Nucleic Acids Res.* **22,** 4673–4680
11. Morin, P., Sagné, C., and Gasnier, B. (2004) Functional characterization of wild-type and mutant human sialin. *EMBO J.* **23,** 4560–4570
12. Wreden, C. C., Wlizla, M., and Reimer, R. J. (2005) Varied mechanisms underlie the free sialic acid storage disorders. *J. Biol. Chem.* **280,** 1408–1416
13. Aula, N., Salomäki, P., Timonen, R., Verheijen, F., Mancini, G., Månsson, J. E., Aula, P., and Peltonen, L. (2000) The spectrum of *SLC17A5* gene mutations resulting in free sialic acid-storage diseases indicates some genotype-phenotype correlation. *Am. J. Hum. Genet.* **67,** 832–840
14. Verheijen, F. W., Verbeek, E., Aula, N., Beerens, C. E., Havelaar, A. C., Joosse, M., Peltonen, L., Aula, P., Galjaard, H., van der Spek, P. J., and Mancini, G. M. (1999) A new gene, encoding an anion transporter, is mutated in sialic acid storage diseases. *Nat. Genet.* **23,** 462–465
15. Aula, N., Jalanko, A., Aula, P., and Peltonen, L. (2002) Unraveling the molecular pathogenesis of free sialic acid storage disorders: altered targeting of mutant sialin. *Mol. Genet. Metab.* **77,** 99–107
16. Fan, J. Q. (2008) A counterintuitive approach to treat enzyme deficiencies: use of enzyme inhibitors for restoring mutant enzyme activity. *Biol. Chem.* **389,** 1–11
17. Miyaji, T., Echigo, N., Hiasa, M., Senoh, S., Omote, H., and Moriyama, Y. (2008) Identification of a vesicular aspartate transporter. *Proc. Natl. Acad. Sci. U.S.A.* **105,** 11720–11724
18. Bardor, M., Nguyen, D. H., Diaz, S., and Varki, A. (2005) Mechanism of uptake and incorporation of the non-human sialic acid *N*-glycolylneuraminic acid into human cells. *J. Biol. Chem.* **280,** 4228–4237
19. Varki, A. (2010) Colloquium paper: uniquely human evolution of sialic acid genetics and biology. *Proc. Natl. Acad. Sci. U.S.A.* **107,** Suppl. 2, 8939–8946
20. Byres, E., Paton, A. W., Paton, J. C., Löfling, J. C., Smith, D. F., Wilce, M. C., Talbot, U. M., Chong, D. C., Yu, H., Huang, S., Chen, X., Varki, N. M., Varki, A., Rossjohn, J., and Beddoe, T. (2008) Incorporation of a non-human glycan mediates human susceptibility to a bacterial toxin. *Nature* **456,** 648–652
21. Chaudhry, F. A., Edwards, R. H., and Fonnum, F. (2008) Vesicular neurotransmitter transporters as targets for endogenous and exogenous toxic substances. *Annu. Rev. Pharmacol. Toxicol.* **48,** 277–301
22. Pietrancosta, N., Kessler, A., Favre-Besse, F. C., Triballeau, N., Quentin, T., Giros, B., El Mestikawy, S., and Acher, F. C. (2010) Rose Bengal analogues and vesicular glutamate transporters (VGLUTs). *Bioorg. Med. Chem.* **18,** 6922–6933
23. Thompson, C. M., Davis, E., Carrigan, C. N., Cox, H. D., Bridges, R. J., and Gerdes, J. M. (2005) Inhibitor of the glutamate vesicular transporter (VGLUT). *Curr. Med. Chem.* **12,** 2041–2056
24. Huang, Y., Lemieux, M. J., Song, J., Auer, M., and Wang, D. N. (2003) Structure and mechanism of the glycerol-3-phosphate transporter from *Escherichia coli*. *Science* **301,** 616–620
25. Meindl, P., and Tuppy, H. (1965) [Synthetic ketosides of *N*-acetyl-D-neuraminic acid. I. Characterization of a series of neuraminidase-cleavable ketosides]. *Monatshefte für Chemie* **96,** 802–815
26. Kuhn, R., Lutz, P., and MacDonald, D. L. (1966) [Synthesis of the anomer sialic acid-methylketoside]. *Chem. Ber.* **99,** 611–617
27. Meindl, P., and Tuppy, H. (1969) [2-Deoxy-2,3-dehydro-sialic acids. I. Synthesis and properties of 2-deoxy-2,3-dehydro-*N*-acyl-neuraminic acids and their methyl esters]. *Monatshefte für Chemie* **100,** 1295–1306
28. Gross, H. J., and Brossmer, R. (1988) Inhibition of *N*-acetylneuraminate lyase by *N*-acetyl-4-oxo-D-neuraminic acid. *FEBS Lett.* **232,** 145–147
29. Baumberger, F., and Vasella, A. (1986) 16th communication: synthesis of *N*-acetyl-4-deoxyneuraminic acid. *Helvet. Chim. Acta* **69,** 1535–1541
30. Hagedorn, H. W., and Brossmer, R. (1986) Synthesis and biological properties of *N*-acetyl-4-deoxy-D-neuraminic acid. *Helvet. Chim. Acta* **69,** 2127–2132
31. Ogura, H., Furuhata, K., Sato, S., Anazawa, K., Itoh, M., and Shitori, Y. (1987) Synthesis of 9-*O*-acyl- and 4-*O*-acetyl-sialic acids. *Carbohydr. Res.* **167,** 77–86
32. Mack, H., and Brossmer, R. (1998) [Chain lengthening of 1-deoxy-1-nitroalditols by nitrile oxide cycloaddition: synthesis of 4-*N*-substituted 3,4-dideoxy-2-ulosonic acids]. *Tetrahedron* **54,** 4539–4560
33. Meindl, P., and Tuppy, H. (1966) [Characterization and enzymatic cleavage of α-ketosides of *N*-propionyl-, *N*-butyryl, and *N*-benzoyl-D-neuraminic acids]. *Monatshefte für Chemie* **97,** 1628–1647
34. Humphrey, A. J., Fremann, C., Critchley, P., Malykh, Y., Schauer, R., and Bugg, T. D. (2002) Biological properties of *N*-acyl and *N*-haloacetyl neuraminic acids: processing by enzymes of sialic acid metabolism and interaction with influenza virus. *Bioorg. Med. Chem.* **10,** 3175–3185
35. Kelm, S., Schauer, R., Manuguerra, J. C., Gross, H. J., and Crocker, P. R. (1994) Modifications of cell surface sialic acids modulate cell adhesion mediated by sialoadhesin and CD22. *Glycoconj. J.* **11,** 576–585
36. Brossmer, R., and Gross, H. J. (1994) Sialic acid analogues and application for preparation of neoglycoconjugates. *Methods Enzymol.* **247,** 153–176
37. Schauer, R., Wirtz-Peitz, F., and Faillard, H. (1970) [Synthesis of *N*-acylneuraminic acids. II. *N*-[1-^{14}C]glycolyl-, *N*-chloroacetyl- and *N*-fluoroacetylneuraminic acids]. *Hoppe Seylers Z. Physiol. Chem.* **351,** 359–364
38. Oetke, C., Brossmer, R., Mantey, L. R., Hinderlich, S., Isecke, R., Reutter, W., Keppler, O. T., and Pawlita, M. (2002) Versatile biosynthetic engineering of sialic acid in living cells using synthetic sialic acid analogues. *J. Biol.*

Chem. **277,** 6688–6695
39. Isecke, R., and Brossmer, R. (1995) Synthesis of *N*-acetyl-9-S-acetyl-9-thioneuraminic acid, *N*-acetyl-9-thioneuraminic acid, and their methyl α-glycosides. *Carbohydr. Res.* **274,** 303–311
40. Brossmer, R., Rose, U., Kaspar, D., Smith, T. L., Grasmuk, H., and Unger, F. M. (1980) Enzymic synthesis of 5-acetamido-9-azido-3,5,9-trideoxy-D-glycero-D-galacto-2-nonulosonic acid, a 9-azido-9-deoxy derivative of *N*-acetylneuraminic acid. *Biochem. Biophys. Res. Commun.* **96,** 1282–1289
41. Isecke, R., and Brossmer, R. (1994) Synthesis of 5-*N*-thioacylated and 9-*N*-thioacylated sialic acids. *Tetrahedron* **50,** 7445–7460
42. Zbiral, E., Brandstetter, H. H., and Schreiner, E. P. (1988) [Structural transformations of *N*-acetyl-neuraminic acid. 8. Synthesis of 7-deoxy-neuraminic, 8-deoxy-neuraminic, 9-deoxy-neuraminic, and 4,7-dideoxy-neuraminic acids]. *Monatshefte für Chemie* **119,** 127–141
43. Gross, H. J., Bünsch, A., Paulson, J. C., and Brossmer, R. (1987) Activation and transfer of novel synthetic 9-substituted sialic acids. *Eur. J. Biochem.* **168,** 595–602
44. Kiefelt, M. J., Wilson, J. C., Bennett, S., Gredley, M., and von Itzstein, M. (2000) Synthesis and evaluation of C-9 modified *N*-acetylneuraminic acid derivatives as substrates for *N*-acetylneuraminic acid aldolase. *Bioorg. Med. Chem.* **8,** 657–664
45. Auge, C., David, S., Gautheron, C., Malleron, A., and Cavaye, B. (1988) Preparation of six naturally-occurring sialic acids with immobilized acylneuraminate pyruvate lyase. *New J. Chem.* **12,** 733–744
46. Krogh, A., Larsson, B., von Heijne, G., and Sonnhammer, E. L. (2001) Predicting transmembrane protein topology with a hidden Markov model: application to complete genomes. *J. Mol. Biol.* **305,** 567–580
47. Tusnády, G. E., and Simon, I. (2001) The HMMTOP transmembrane topology prediction server. *Bioinformatics* **17,** 849–850
48. Wu, G., Robertson, D. H., Brooks, C. L., 3rd, and Vieth, M. (2003) Detailed analysis of grid-based molecular docking: A case study of CDOCKER-A CHARMm-based MD docking algorithm. *J. Comput. Chem.* **24,** 1549–1562
49. Kirchmair, J., Laggner, C., Wolber, G., and Langer, T. (2005) Comparative analysis of protein-bound ligand conformations with respect to catalyst's conformational space subsampling algorithms. *J. Chem. Inf. Model* **45,** 422–430
50. Wallace, A. C., Laskowski, R. A., and Thornton, J. M. (1995) LIGPLOT: a program to generate schematic diagrams of protein-ligand interactions. *Protein Eng.* **8,** 127–134
51. Lovell, S. C., Davis, I. W., Arendall, W. B., 3rd, de Bakker, P. I., Word, J. M., Prisant, M. G., Richardson, J. S., and Richardson, D. C. (2003) Structure validation by Cα geometry: φ, ψ, and Cβ deviation. *Proteins* **50,** 437–450
52. Irwin, J. J., and Shoichet, B. K. (2005) ZINC: a free database of commercially available compounds for virtual screening. *J. Chem. Inf. Model* **45,** 177–182
53. Yin, Y., He, X., Szewczyk, P., Nguyen, T., and Chang, G. (2006) Structure of the multidrug transporter EmrD from *Escherichia coli*. *Science* **312,** 741–744
54. Bajorath, J. (2002) Integration of virtual and high-throughput screening. *Nat. Rev. Drug Discov.* **1,** 882–894
55. Aramori, I., Nirei, H., Shoubo, M., Sogabe, K., Nakamura, K., Kojo, H., Notsu, Y., Ono, T., and Nakanishi, S. (1993) Subtype selectivity of a novel endothelin antagonist, FR139317, for the two endothelin receptors in transfected Chinese hamster ovary cells. *Mol. Pharmacol.* **43,** 127–131
56. Courville, P., Quick, M., and Reimer, R. J. (2010) Structure-function studies of the SLC17 transporter sialin identify crucial residues and substrate-induced conformational changes. *J. Biol. Chem.* **285,** 19316–19323
57. Juge, N., Yoshida, Y., Yatsushiro, S., Omote, H., and Moriyama, Y. (2006) Vesicular glutamate transporter contains two independent transport machineries. *J. Biol. Chem.* **281,** 39499–39506
58. Almqvist, J., Huang, Y., Laaksonen, A., Wang, D. N., and Hovmöller, S. (2007) Docking and homology modeling explain inhibition of the human vesicular glutamate transporters. *Protein Sci.* **16,** 1819–1829
59. Du, J., Meledeo, M. A., Wang, Z., Khanna, H. S., Paruchuri, V. D., and Yarema, K. J. (2009) Metabolic glycoengineering: sialic acid and beyond. *Glycobiology* **19,** 1382–1401
60. Prescher, J. A., Dube, D. H., and Bertozzi, C. R. (2004) Chemical remodeling of cell surfaces in living animals. *Nature* **430,** 873–877
61. Saxon, E., and Bertozzi, C. R. (2000) Cell surface engineering by a modified Staudinger reaction. *Science* **287,** 2007–2010
62. Gubernator, N. G., Zhang, H., Staal, R. G., Mosharov, E. V., Pereira, D. B., Yue, M., Balsanek, V., Vadola, P. A., Mukherjee, B., Edwards, R. H., Sulzer, D., and Sames, D. (2009) Fluorescent false neurotransmitters visualize dopamine release from individual presynaptic terminals. *Science* **324,** 1441–1444
63. Pawlita, M., Oetke, C., Keppler, O., Brossmer, R., Hinderlich, S., and Reutter, W. (February 27, 2003) Glycoconjugates of sialic acid derivates, methods for their production and use thereof, World Intellectual Property Organization Patent WO/2003/016329